NATIONAL ADVISORY COMMITTEE FOR AERONAUTICS

TECHNICAL NOTE

No. 1551

FRACTURE STRENGTH OF 75S-T ALUMINUM ALLOY UNDER COMBINED STRESS

By E. G. Thomsen, I. Lotze, and J. E. Dorn

University of California

Washington

July 1948

NATIONAL ADVISORY COMMITTEE FOR AERONAUTICS

TECHNICAL NOTE NO. 1551

FRACTURE STRENGTH OF 75S-T ALUMINUM ALLOY UNDER COMBINED STRESS

By E. G. Thomsen, I. Lotze, and J. E. Dorn

SUMMARY

The effect of combined stresses on the fracture strength of 75S-T aluminum alloy was determined by applying axial loads and internal pressure to thin-wall drawn tubes. Tubular extrusions of 75S-T aluminum alloy rupture in substantial agreement with the critical shear stress law for fracture. Values of the shear stress for fracture are greater when the macroscopic plane of fracture cuts the lines of fibering than they are when the plane of fracture is parallel to the directions of maximum principal extension during fabrication. As the mean hydrostatic tension increases, the critical shear stress for fracture appears to decrease. The effects of other factors on the fracture strength of 75S-T aluminum alloy are discussed.

INTRODUCTION

Investigations leading to knowledge of the conditions under which alloys will fracture have broad scientific and engineering interest. The importance of this subject in aircraft engineering stems from two objectives: (1) To design parts that will not fracture during fabrication, and (2) to design aircraft structures that will not fracture in service. As higher strength materials are used in order to provide lighter weight structures, it becomes increasingly important to have detailed knowledge of the factors affecting their fracture strength.

Several extensive surveys (references 1 to 3) on the phenomenon of fracture have been reported recently. These reviews reveal that the effect of combined stresses is one of the most important factors affecting the fracture strength of metals; but other factors, such as previous strain history, temperature, and strain rate, also influence the fracture strength of metals. In general, however, the data on fracture phenomena are unsatisfactorily incomplete and much additional information is required before the laws of fracture can be used with confidence to determine forming limits and design criterions for aircraft structures.

Preliminary data on the effect of biaxial stresses on the fracture strength of several aircraft materials have been reported in the literature. Tubular extrusions of magnesium alloys, FS-1, J-1, and O-1, give

the true fracture stresses (true stress is defined as the load divided by the instantaneous cross-sectional area) shown in figures 1 to 3 (reference 4). Drawn tubes of 24S-T, 24S-T80, and 24S-T81 alloys reveal somewhat the same trend, as shown in figures 4 to 6 (reference 5). Increased interest on behalf of aeronautical engineers in the use of 75S-T aluminum alloy indicated the need for obtaining parallel data on this material.

This work was conducted at the University of California under the sponsorship and with the financial assistance of the National Advisory Committee for Aeronautics. The authors acknowledge the important contributions of Mr. W. Pemberton in preparing accurate specimens for test and they thank Messrs. T. Robinson and J. McChesney for their assistance in conducting the tests. To Dean M. P. O'Brien they extend their appreciation for his interest and continued support of these investigations.

SYMBOLS

τ_{zz} true stress in axial direction of tube

$\tau_{\theta\theta}$ true stress in hoop direction of tube

τ_{rr} true stress in radial direction of tube

τ_{11}, τ_{22}, τ_{33} maximum, intermediate, and minimum principal stresses, respectively

$\bar{\sigma}$ effective stress

$$\left(\sqrt{\frac{(\tau_{11}-\tau_{22})^2+(\tau_{22}-\tau_{33})^2+(\tau_{33}-\tau_{11})^2}{2}}\right)$$

$\bar{\phi}$ effective strain

$$\left(\int \frac{2}{3}\sqrt{\frac{(\epsilon_{11}-\epsilon_{22})^2+(\epsilon_{22}-\epsilon_{33})^2+(\epsilon_{33}-\epsilon_{11})^2}{2}}\right)$$

$\bar{\sigma}_0$ effective stress at yielding

P applied pressure

r_i, r_o instantaneous inner and outer radii of tube, respectively

$(\tau_s)_{cr}$ critical shear stress at fracture

ϵ_{11}, ϵ_{22}, ϵ_{33} infinitesimal strains in principal directions

SPECIMENS AND MATERIAL

The conventional method for obtaining a wide range of substantially biaxial stresses by subjecting thin-wall tubular specimens to internal pressure and axial loading was adopted in this investigation. Specimens shown in figure 7 were prepared from drawn tubes of 75S-T aluminum alloy having an internal diameter of 3.6 inches and a wall thickness of 0.45 inch. The inner wall was carefully machined to provide a smooth surface; the outer surface of the specimen was machined on a tight-fitting mandrel in order to maintain concentricity of the inner and outer surfaces. The variation in wall thickness was less than about 0.001 inch. After machining, the outer surface was polished parallel to the direction of maximum principal stress with 2/0 emery paper. The nominal composition of 75S-T alloy is given in percentages as follows:

Copper	1.6
Manganese	0.2
Magnesium	2.5
Zinc	5.6
Chromium	0.03

In order to permit comparison with 75S-T sheet material, standard A.S.T.M. tensile specimens, 1/2 inch wide and 0.125 inch thick, were prepared from blanks selected parallel to the direction of drawing. These data are given as follows:

Yield strength, psi	83,400
Tensile strength, psi	95,000
Elongation per inch, percent	15
Reduction in area, percent	30

A typical fabrication sequence for 75S-T drawn tubing is shown as follows:

Extrusion:
Ingot is extruded at annealing temperature and cooled to room temperature in air. Condition, 75S-O.

Drawing:
Extruded tubing is drawn through die over mandrel to approximate size. Condition, 75S-As.

Solution heat treatment:
Tube is heated to 860° to 930° F and quenched in cold water. Condition, 75S-W.

Precipitation hardening:

Two methods may be used –

(a) Tube is heated to 245° to 255° F, held for 22 to 26 hours, and cooled in air to room temperature.

(b) Tube is heated to 205° to 215° F, held for 4 to 6 hours, and cooled in air to room temperature.

The tube is reheated to 310° to 320° F, held for 8 to 10 hours, and cooled in air to room temperature. Condition, 75S–T.

Straightening:

Tubing that has warped during heat treatment may be straightened by several methods, such as,

(a) Stretch straightening

(b) Roll straightening

(c) Cold drawing a few light passes

Although the data contained in this report on the fracture strength of 75S–T alloy pertain only to the drawn tubes which were investigated, it is logical to assume that other forms of this alloy will yield analogous effects of combined stresses on their fracture strength.

Because of buckling, the tubular specimens were unsatisfactory for determining the fracture conditions for ratios of axial compression to circumferential tension greater than about 1 to 2. In order to obtain fracture data for axial and circumferential compression, small cylindrical compression specimens having a diameter and height of 0.04 inch were prepared. The fracture stresses in compression obtained from these 75S–T drawn tubes are: in the longitudinal direction of stressing, 116,600 psi and 120,000 psi; and in the circumferential direction of stressing, 120,000 psi and 120,000 psi.

EXPERIMENTAL TECHNIQUE AND RESULTS

The tubular specimens were held in grips especially designed to insure oil tightness and alinement during loading; the details of technique have been described in an earlier report (reference 5). Axial tension or compression loading was applied with a 200,000–pound Tate–Emery hydraulic–type testing machine. The internal pressure was obtained with a two–cylinder fuel oil injection pump so modified as to give steady pressures. The applied pressures were measured with carefully calibrated Bourdon type pressure gages, which were checked periodically with an American gage–tester.

Internal pressures and axial loads were applied to the tubular specimens in such a way that the ratio of true axial stress to true hoop stress remained approximately constant up to fracture. In order to maintain constant stress ratios, it was necessary to readjust the ratio of load and pressure periodically. The method consisted in loading the specimen at a predetermined ratio of pressure to maximum load in an

initial step. After this load was reached the pressure and axial load were simultaneously decreased to zero. The dimensions of the tube were then measured at zero load. From the dimensions of the plastically deformed tube the new ratio of pressure and load was obtained from previously prepared curves, and the specimen was reloaded to a new value. This method of adjusted cyclic loading was continued to fracture.

The results on fracture for stress ratios varying from pure axial tension through the biaxial tension–tension region and into the hoop tension–axial compression region are shown in figure 8. Microcompression fracture data have also been included in this figure.

Photographs of typical fractures are shown in figure 9(a) and the types of fracture are indicated in figure 9(b). The macroscopic plane of fracture for magnesium alloys coincided with the plane of maximum shear stress. (See figs. 1 to 3.) In general this trend is also common to aluminum alloys except under combined tension and compression stresses when the aluminum alloys exhibited type–B fracture rather than type–C. Only slight necking was observed when the tubes were tested in pure axial tension. Under the remaining conditions fracture occurred without detectable necking.

The propensity of 75S–T alloy to crack propagation is greater than that of the other aluminum alloys which were previously investigated. Under conditions approaching biaxial tension $\left(\text{e.g., } \frac{\tau_{zz}}{\tau_{\theta\theta}} = \frac{1.1}{1}\right)$ the central section of the tube shattered into a number of fragments.

DISCUSSION

Several laws have been proposed to account for the observed effect of combined stresses on the true fracture strength of metals. On the basis of investigations by Siebel and Maier (reference 6) on the fracture strength of steels, brass, and cast iron under biaxial tension, Gensamer (reference 1) proposed that metals fracture when the maximum principal stress exceeds a critical value. Data on the fracture stress of ductile steels when pulled in tension under hydrostatic pressure prompted Bridgman (reference 7) to suggest that metals fail when a critical value of the mean hydrostatic tension is reached. Thomsen, Cunningham, and Dorn (references 4 and 5) have presented evidence that some magnesium and aluminum alloys fracture when the maximum shear stress reaches a critical value. The idealized diagram of the fracture stresses over the field of biaxial stressing for each of these laws is shown in figure 10. The experimental data for the fracture of 75S–T alloy, shown in figure 8, agree best with the trends required by the maximum shear stress law.

The available evidence purporting to support the maximum principal stress law is weak. Tests by Siebel and Maier (reference 6) were

confined to the tension–tension quadrant of biaxial stresses, where the trends of the fracture stress are identical for the maximum principal stress law and maximum shear stress law. Furthermore, the materials which Siebel and Maier studied, except cast iron, were highly ductile and necked markedly before fracturing. Therefore the precise state of stress in the necked region may have differed appreciably from the average values which were reported.

Cook and Robertson (reference 8) investigated the fracture strength of thick–wall cylinders of cast iron in the tension–compression region of stresses where clear delineation between the three proposed laws is obtained. Although their results may not be definitive because of the unknown effects of stress gradients in the thick–wall tubes, the data are nevertheless given in figure 11 for comparison. These data suggest that over the range of stresses which was investigated, cast iron fractures in fair agreement with the maximum principal stress law. This conclusion is not inconsistent with the data reported by Siebel and Maier (reference 6) and also that presented by Ros and Eichinger (reference 9) for the fracture of cast iron under biaxial tension. Cast iron, however, is known to fracture on planes of maximum shear stress at values of compressive stress equal to about four to six times the tensile stress necessary to cause fracture. It has been suggested, therefore, that cast iron may fracture in accordance with either a maximum shear stress law or a maximum principal stress law, as illustrated in figure 11, depending upon which critical value is exceeded first.

Although the existing data on the fracture of metals under biaxial stresses do not agree with the hydrostatic–tension stress law, the possible importance of hydrostatic tension on fracture cannot be overlooked. Recent discussions by McAdam (reference 10) on the fracture of severely notched tension bars suggest that the critical condition for fracture may be a function of the hydrostatic tension. If a maximum shear stress law be admitted, according to the implications of McAdam's data, the critical shear stress for fracture becomes a function of the hydrostatic tension, as shown schematically in figure 12. According to this picture the critical shear stress for fracture decreases with increasing hydrostatic tension; at an appropriately high value of the mean hydrostatic tension, fracture occurs in the absence of a shear stress, that is, by hydrostatic tension. Although McAdam's conclusions were based on notched–bar tensile data, for which the stress distribution, at present, is only qualitatively determinable, the evidence favoring the proposed general trends of the effect of hydrostatic tension on fracture is substantial. Furthermore the proposed effect of hydrostatic tension on the fracture strength of metals is in qualitative agreement with Bridgman's data on the fracture of necked tensile specimens. The fracture data for magnesium alloys, shown in figures 1 to 3, however, indicate that the hydrostatic tension does not influence the critical shear stress at fracture and that the deviations of the experimental points from the ideal critical shear diagram for fracture must be due to another cause.

The fracture strength also appears to be a function of the amount of work–hardening preceding fracture (reference 3). Sakharov (reference 11) and Zener and Hollomon (references 12 and 13) have demonstrated

that the tensile fracture strength of steel (at temperatures sufficiently low to yield substantially brittle fracture) increases with prestrain at atmospheric temperatures. The effect of prestraining appears to account for the cusps observed in the fracture strength of magnesium alloys (figs. 1 to 3). As indicated in figure 13, the effective stress for plastic flow (reference 2) $\bar{\sigma} = \sqrt{\frac{(\tau_{11} - \tau_{22})^2 + (\tau_{22} - \tau_{33})^2 + (\tau_{33} - \tau_{11})^2}{2}}$ for equivalent amounts of work-hardening for an isotropic material is a series of ellipses with their major axes at 45° to the two principal stresses in the biaxial region of stresses. As the metal is work-hardened the flow stress increases from $\bar{\sigma}_0$, the yield strength, to higher values $\bar{\sigma}_1$, and so forth. Finally a value is reached, for example $\bar{\sigma}_2$, which intersects the fracture curve (assumed here to be a shear stress curve) at $\frac{\tau_{11}}{\tau_{22}} = \frac{4}{2}$, $\frac{\tau_{11}}{\tau_{22}} = \frac{2}{4}$, and $\frac{\tau_{11}}{\tau_{22}} = -\frac{2}{4}$, resulting in fracture at these points. In order to induce fracture for the stress ratio $\frac{\tau_{11}}{\tau_{22}} = \frac{4}{4}$ the metal must be work-hardened an additional amount corresponding to an enlargement of the flow ellipse from point a to point b. The same analysis applies to stress ratios $\frac{\tau_{11}}{\tau_{22}} = \frac{4}{0}$, $\frac{\tau_{11}}{\tau_{22}} = \frac{0}{4}$, and $\frac{\tau_{11}}{\tau_{22}} = -\frac{4}{0}$. If the critical shear stress for fracture increases with work-hardening, the fracture stress curve then becomes cusped at the foregoing stress ratios, as reported in figures 1 to 3, for magnesium alloys. The effect of strain on the fracture stress of J-1 alloy is illustrated in figure 14. It appears from the average curve drawn through the scatter band that the critical shear stress for fracture increases as the effective strain $\bar{\phi}$ increases. ($\bar{\phi} = \int \frac{2}{3} \sqrt{\frac{(\epsilon_{rr} - \epsilon_{\theta\theta})^2 + (\epsilon_{\theta\theta} - \epsilon_{zz})^2 + (\epsilon_{zz} - \epsilon_{rr})^2}{2}}$ where ϵ_{rr}, $\epsilon_{\theta\theta}$, and ϵ_{zz} are infinitesimal strains on fibers in the radial, circumferential, and axial directions, respectively. According to the idealized theory of plasticity of work-hardenable metals, $\bar{\sigma}$ is a function of $\bar{\phi}$. This relation is determinable from a tension test when $\bar{\sigma} = \tau_{zz}$ and $\bar{\phi} = \log_e l_0/l$, where l_0 and l are the initial and instantaneous gage lengths, respectively. Thus the $\bar{\sigma} - \bar{\phi}$ curve is merely the true stress-true strain curve in tension.)

The evidence for the fracture of 75S-T alloy under substantially biaxial stressing as presented in figure 8 may now be critically reviewed in terms of the previous discussion. The reported points represent the true stresses at fracture obtained from the thin-wall-tube formulas

$$\tau_{zz} = \frac{P\pi r_i^2 + L}{\pi\left(r_o^2 - r_i^2\right)} \tag{1}$$

$$\tau_{\theta\theta} = \frac{Pr}{t} \tag{2}$$

$$\tau_{rr} = 0 \quad \text{at} \quad r = r_o \tag{3a}$$

$$\tau_{rr} = -P \quad \text{at} \quad r = r_i \tag{3b}$$

where τ_{zz} and $\tau_{\theta\theta}$ are plotted in the diagram. For the range where $\tau_{zz} > \tau_{\theta\theta}$ the maximum shear stress at fracture is

$$(\tau_s)_{cr} = \frac{\tau_{zz} + P}{2} \tag{4}$$

On assuming that $(\tau_s)_{cr}$ can be obtained from the tube tests in simple tension,

$$\tau_{zz} = 2(\tau_s)_{cr} - P = 107{,}500 - P \tag{5}$$

Thus as P increases, the value for τ_{zz} at fracture decreases, as shown by the dashed line of figure 8. Over the range of the tension–tension quadrant of stresses where $\tau_{\theta\theta} > \tau_{zz}$

$$(\tau_s)_{cr} = \frac{\tau_{\theta\theta} + P}{2} \tag{6}$$

and the circumferential stress at fracture becomes

$$\tau_{\theta\theta} = 2(\tau_s)_{cr} - P \tag{7}$$

But since the pressure at fracture remains fairly constant over this range of values, $\tau_{\theta\theta}$ for fracture becomes a vertical line. On using the value of $2(\tau_s)_{cr} = 107{,}500$ as suggested by the tension data for the tubes, the vertical dashed line is obtained. This line, however, continues below $\tau_{zz} = 0$ since τ_{rr} remains the minimum principal stress until $\tau_{zz} = -P$. Below this value of τ_{zz}, $\tau_{\theta\theta}$ is the maximum and τ_{zz} is the minimum principal stress. Therefore, according to an idealized shear stress law, in this region,

$$(\tau_s)_{cr} = \frac{\tau_{\theta\theta} - \tau_{zz}}{2}$$

and, on assuming $2(\tau_s)_{cr}$ to be 107,500 psi as obtained from the tension data, the 45° dashed line of figure 8 is obtained.

The proposed idealized shear stress diagram for the fracture of 75S-T alloy in general agrees sufficiently well with the observed experimental trends to suggest that 75S-T alloy ruptures in accordance with the critical maximum shear stress law. The agreement, however, is far from perfect and the deviations of the theory from the facts demand detailed consideration:

(1) The principal discrepancy between the theory and the facts occurs in the tension-tension quadrant of biaxial stressing. Although the theory suggests that the longitudinal fracture stress over ratios from $\frac{\tau_{zz}}{\tau_{\theta\theta}} = \frac{4}{0}$ to $\frac{\tau_{zz}}{\tau_{\theta\theta}} = \frac{4}{4}$ should be nominally equal to the circumferential fracture stress over ratios from $\frac{\tau_{zz}}{\tau_{\theta\theta}} = \frac{4}{4}$ to $\frac{\tau_{zz}}{\tau_{\theta\theta}} = \frac{0}{4}$, the observed circumferential fracture stresses are lower than the longitudinal fracture stresses. Similar observations pertain to other aluminum alloys (figs. 4 to 6) and steels (reference 6). Such results are common and accrue from the effect of mechanical fibering on the fracture strength of metals; the result is an appreciable decrease in the fracture strength when the plane of fracture parallels the direction of fibering.

(2) The observed values of the tensile fracture stress from A.S.T.M. tensile specimens cut from the walls of the tubular specimen are higher than those obtained from tensile tests on the tubes. Two factors possibly contribute to the observed difference:

(a) The sampling of the metal in the tubes and the test bars was somewhat different.

(b) The fracture test coupons exhibited slight necking, whereas the tubes appear to have exhibited less necking when tested in axial tension; under all remaining conditions of test, the tubes fractured without detectable necking.

(3) The critical shear stress for fracture of 75S-T alloy in compression is greater than the corresponding value for tension. Two factors may be responsible for these data:

(a) It is possible that friction between the anvil and the specimen in the compression tests can account for the higher recorded value of the maximum shear stress at fracture in compression than the observed value in tension. Since every precaution was exercised to reduce the frictional effects to a minimum value by adequate lubrication, it is more likely that the observed trend is a real effect.

(b) If the critical shear stress for fracture were solely a function of the previous plastic strain $\bar{\phi}$, the shear stresses for fracture should be identical for tensile and for compressive stressing; but if the critical shear stress for fracture decreases as the mean hydrostatic tension increases, the shear stress for fracture in compression should be greater than the value obtained in tension. The data in figure 15 for the A and C types of fracture which cut across the planes of mechanical fibering lend credence to the concept that the fracture strength may be a function of the mean hydrostatic tension. The scatter and the limited range of mean hydrostatic tension for the type-B fracture do not provide conclusive evidence for the possible effect of the hydrostatic tension on the critical shear stress for fracture when the macroscopic plane of fracture is parallel to the mechanical fibering.

(4) The critical shear stress for fracture may be dependent upon the effective strain $\bar{\phi}$. The data recorded in figure 16 indicate that the observed critical shear stress for fracture of 75S-T alloy actually increases with increase in $\bar{\phi}$; but, in this example, the trend is not due to the direct effect of strain on the fracture stress, for $\bar{\phi}$ at fracture (for the range of conditions investigated) decreases as $\bar{\theta}$ increases. Thus the fracture stress-effective strain trends are attributable to the effect of the mean hydrostatic tension on the fracture stress. Low values of the mean hydrostatic tension increase the fracture stress; this permits greater effective strains at fracture, thus yielding increasing fracture stresses with increasing effective strains.

CONCLUSIONS

Tests to determine the effect of combined stresses on the fracture strength of 75S-T aluminum alloy by applying axial loads and internal pressure to thin-wall drawn tubes have led to the following conclusions:

1. Tubular extrusions of 75S-T aluminum alloy rupture, under biaxial stresses, in substantial agreement with a critical maximum shear stress law for fracture.

2. Mechanical fibering resulting in lower transverse than longitudinal fracture stresses is the primary factor causing deviations between the idealized critical maximum shear stress law and the observed facts.

3. Increasing the mean hydrostatic tension appears to decrease the critical shear stress for fracture when the fracture plane cuts the lines of mechanical fibering. Evidence of the effect of hydrostatic tension on the shear stress for fracture when the plane of fracture is parallel to the lines of mechanical fibering is inconclusive; over the range of hydrostatic tension which was investigated no effect was detected.

4. The critical shear stress for fracture of 75S-T alloy was independent of the effective strain over the range of conditions which was studied.

University of California
Berkeley, Calif., January 20, 1947

REFERENCES

1. Gensamer, M.: Strength of Metals under Combined Stresses. Am. Soc. Metals, 1940, pp. 59–61.

2. Jelinek, J. J., Latter, A. J., Thomsen, E. G., and Dorn, J. E.: Plastic Flows in Metals. OPRD Rep. No. W–200, May 1945.

3. Hollomon, J. H.: The Problem of Fracture. A Report to the Welding Research Council. The Welding Jour., vol. 25, no. 9, Sept. 1946, pp. 534s–583s.

4. Thomsen, E. G., and Dorn, J. E.: The Effect of Combined Stresses on the Ductility and Rupture Strength of Magnesium-Alloy Extrusions. Jour. Aero. Sci., vol. 11, no. 2, April 1944, pp. 125–136.

5. Thomsen, E. G., Cunningham, D. M., and Dorn, J. E.: Study of the Forming Properties of Aluminum Alloy Sheet. Part XIX – Fracture of Some Aluminum Alloys under Biaxial Stresses. OPRD Rep. No. W–225, July 1945.

6. Siebel, E., and Maier, A.: Der Einfluss mehrachsiger Spannungszustände auf das Formänderungsvermögen metallischer Werkstoffe. VDI Zeitschr., vol. 77, no. 51, Dec. 23, 1933, pp. 1345–1349.

7. Bridgman, P. W.: The Shape of the Neck and the Fracture of Tension Specimens. Exp. Rep. No. WAL 111/7–4, Watertown Arsenal Lab., Jan. 1944.

8. Cook, G., and Robertson, T.: The Strength of Thick Hollow Cylinders under Internal Pressure. Engineering, vol. XCII, 1911, pp. 786–789.

9. Ros, M., and Eichinger, A.: Versuche zur Klärung der Frage der Bruchgefahr. Proc. Second Int. Cong. Appl. Mech., 1926, p. 315.

10. McAdam, D. J., Jr.: Fracture of Metals under Combined Stresses. Trans. Am. Soc. Metals, vol. 37, 1946, pp. 538–566.

11. Sakharov, P. S.: Determination of Brittle Strength. Jour. Tech. Phys. USSR, vol. 6, Heft 8, 1936, pp. 1381–1387.

12. Hollomon, J. H., and Zener, C.: Conditions of Fracture of Steel. Trans. Am. Inst. Min. and Met. Eng., vol. 158, 1944, pp. 283–287.

13. Hollomon, J. H.: The Notched-Bar Impact Test. Trans. Am. Inst. Min. and Met. Eng., vol. 158, 1944, pp. 298–327.

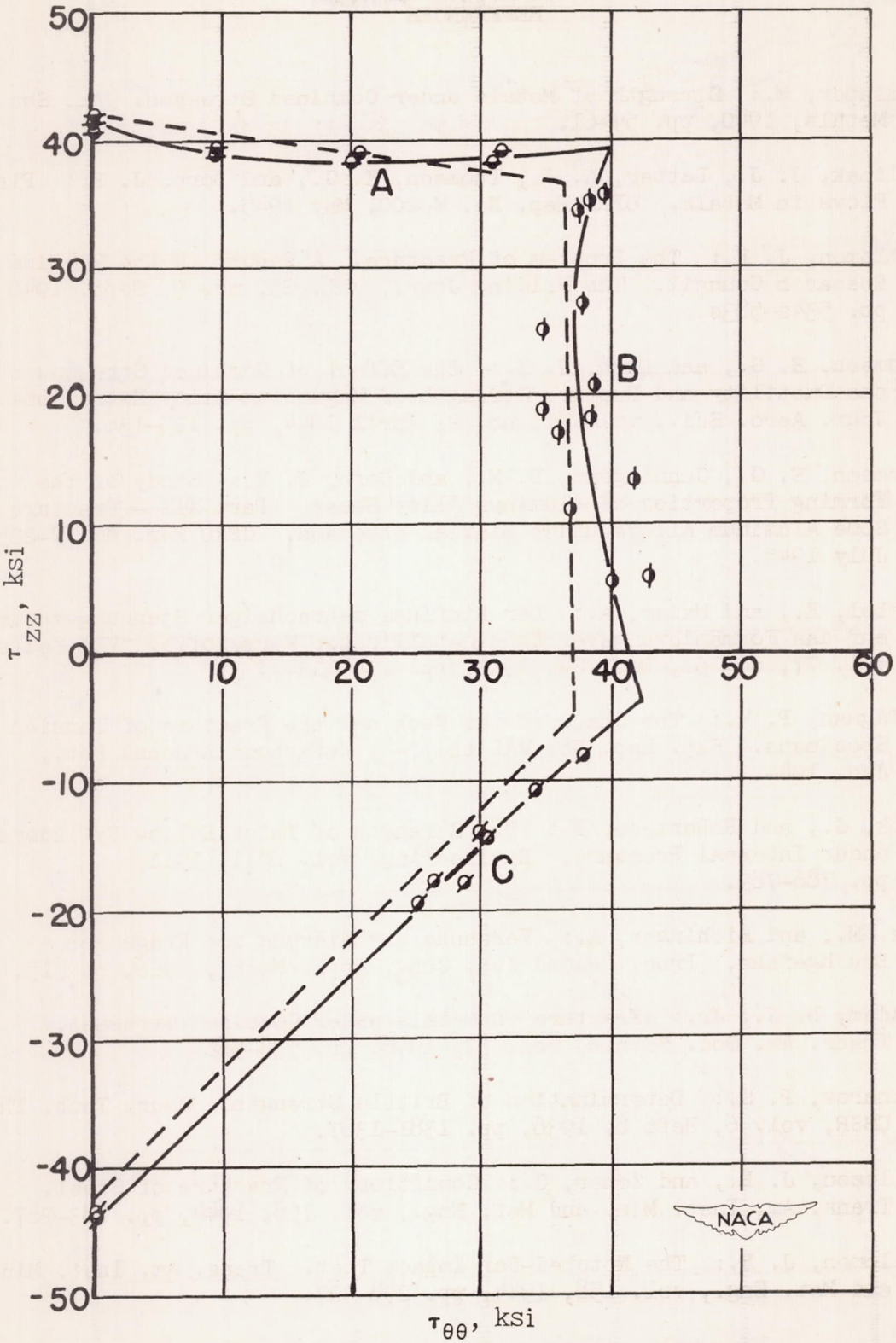

Figure 1.- True stress at fracture for FS-1 magnesium alloy.

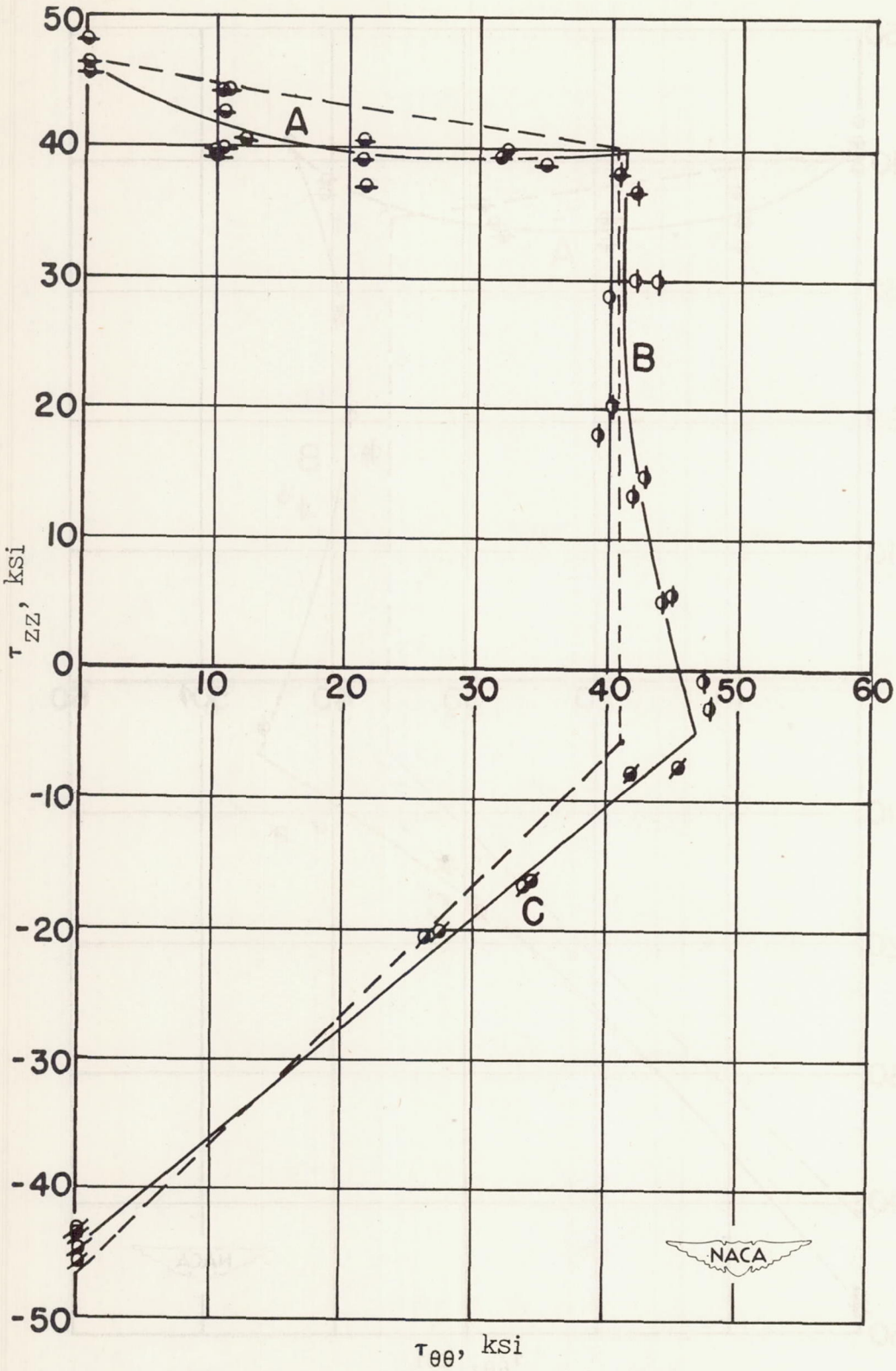

Figure 2.- True stress at fracture for J-1 magnesium alloy.

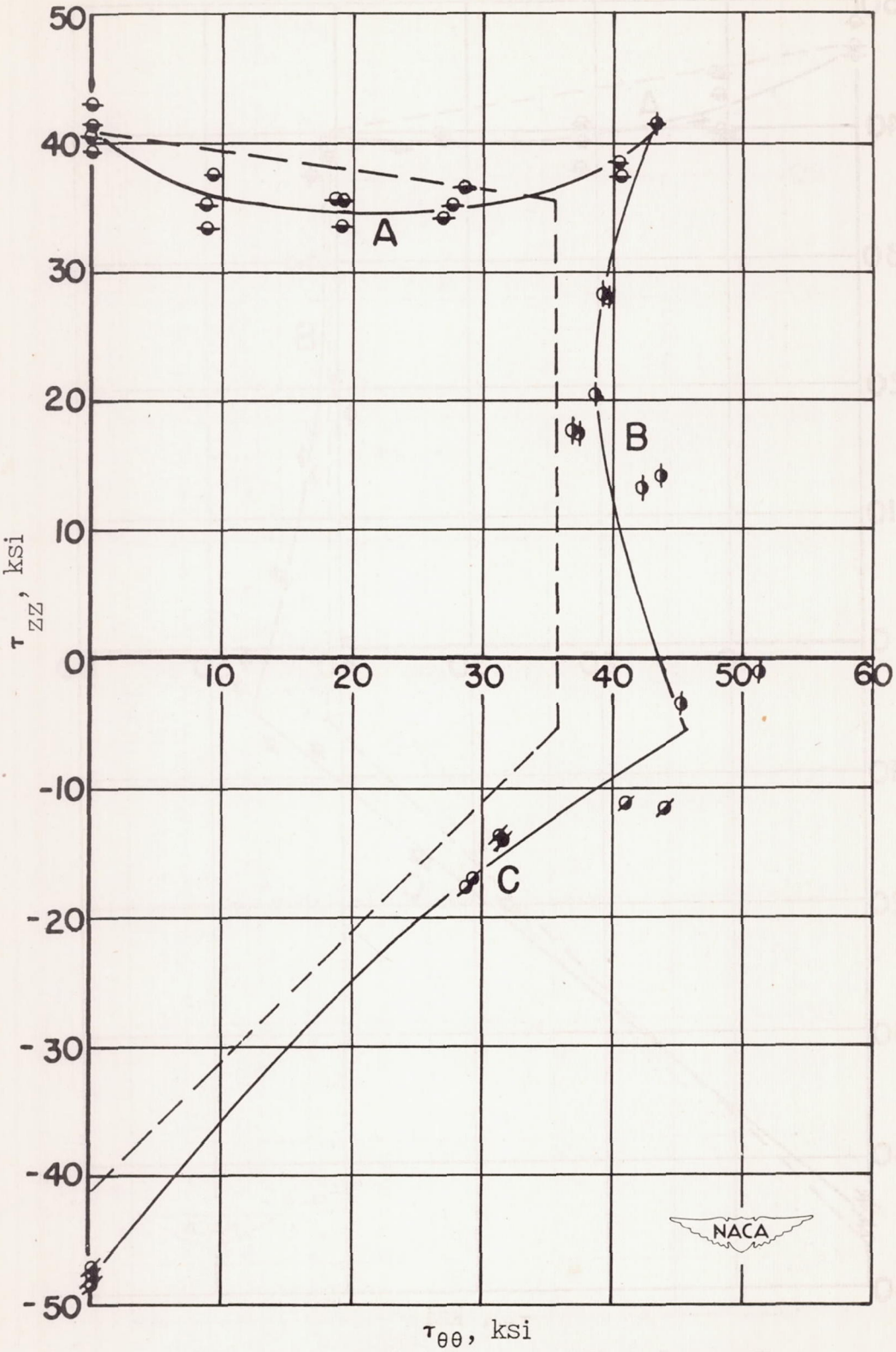

Figure 3.- True stress at fracture for 0-1 magnesium alloy.

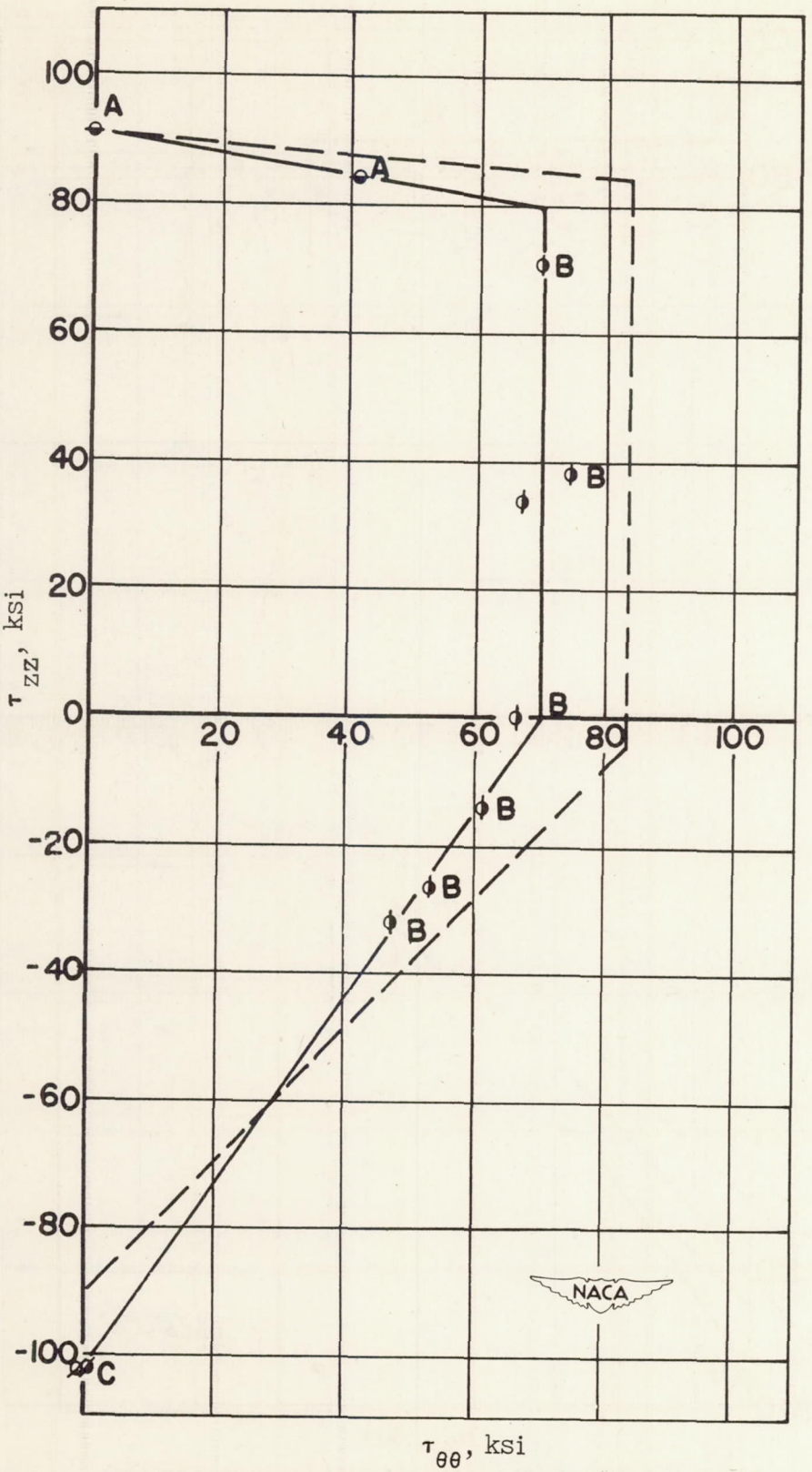

Figure 4.- True stress at fracture for 24S-T aluminum alloy.

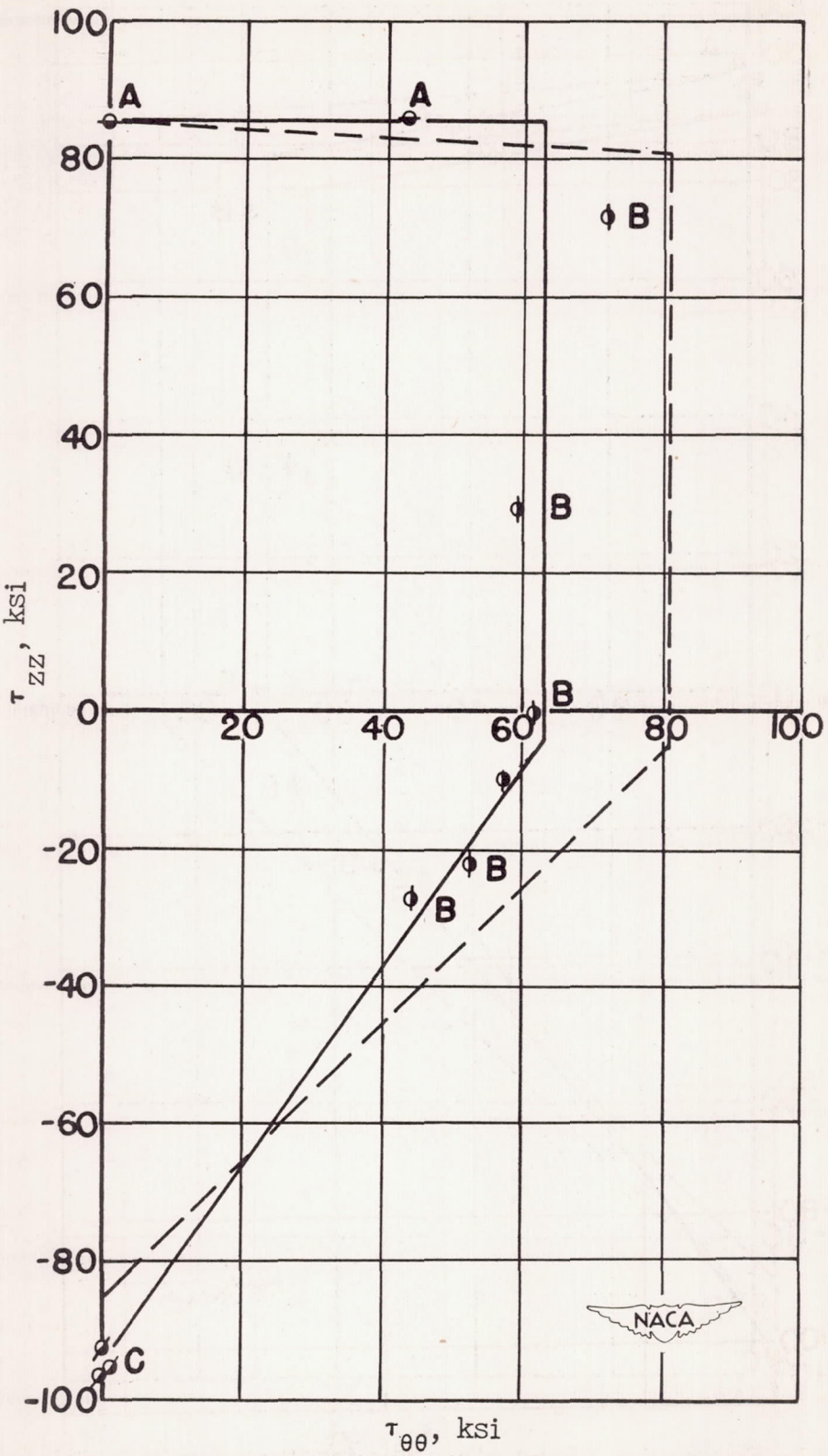

Figure 5.- True stress at fracture for 24S-T80 aluminum alloy.

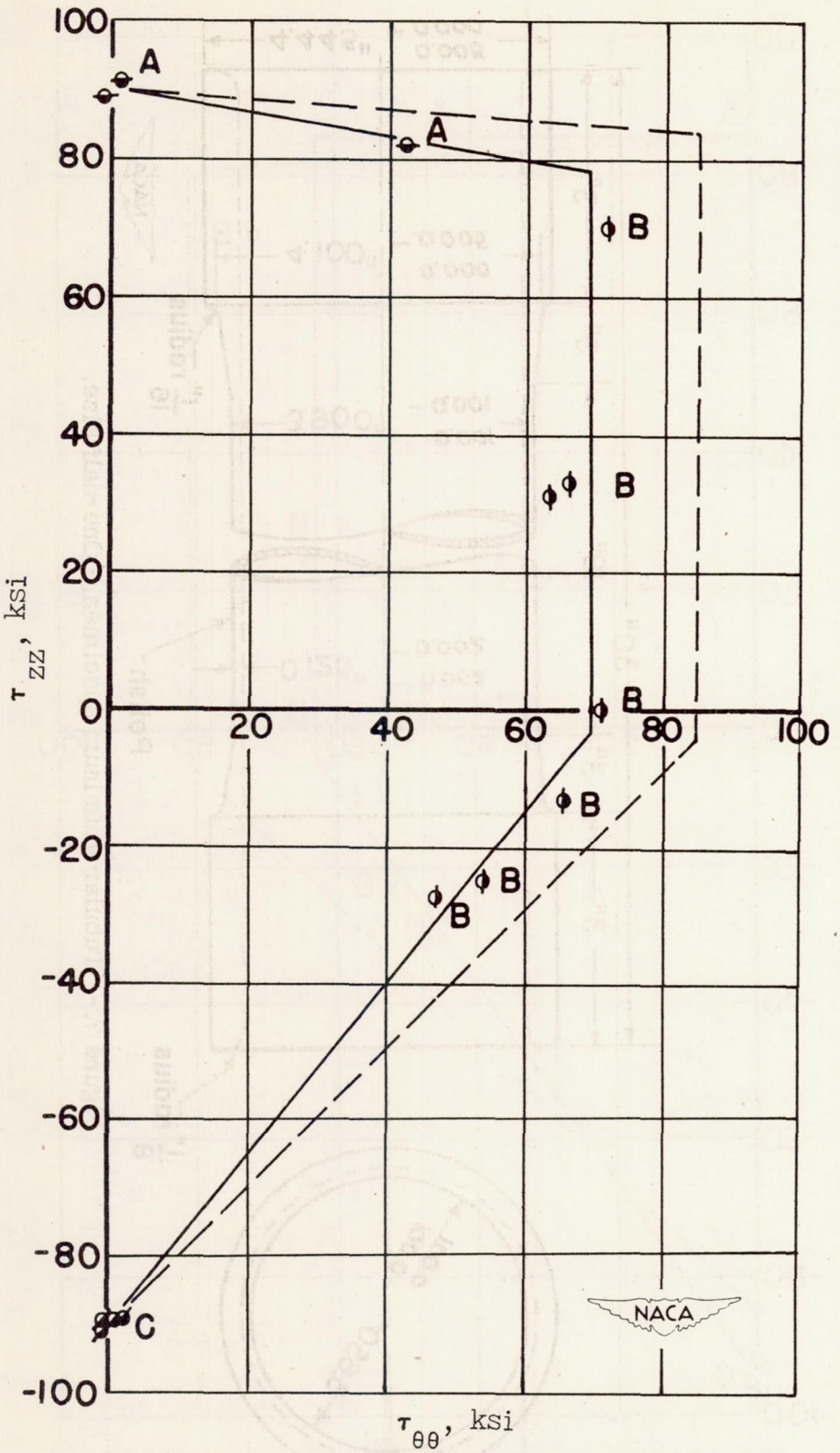

Figure 6.- True stress at fracture for 24S-T81 aluminum alloy.

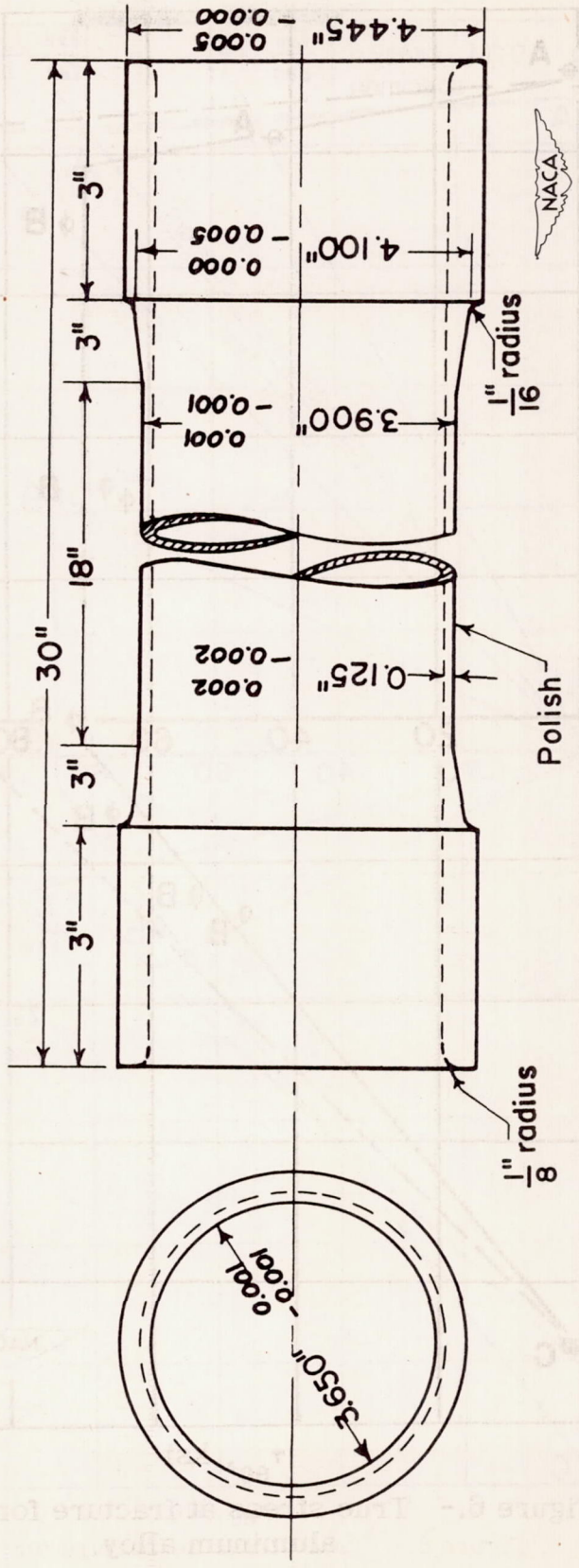

Figure 7.- Tubular aluminum specimen. One-half size.

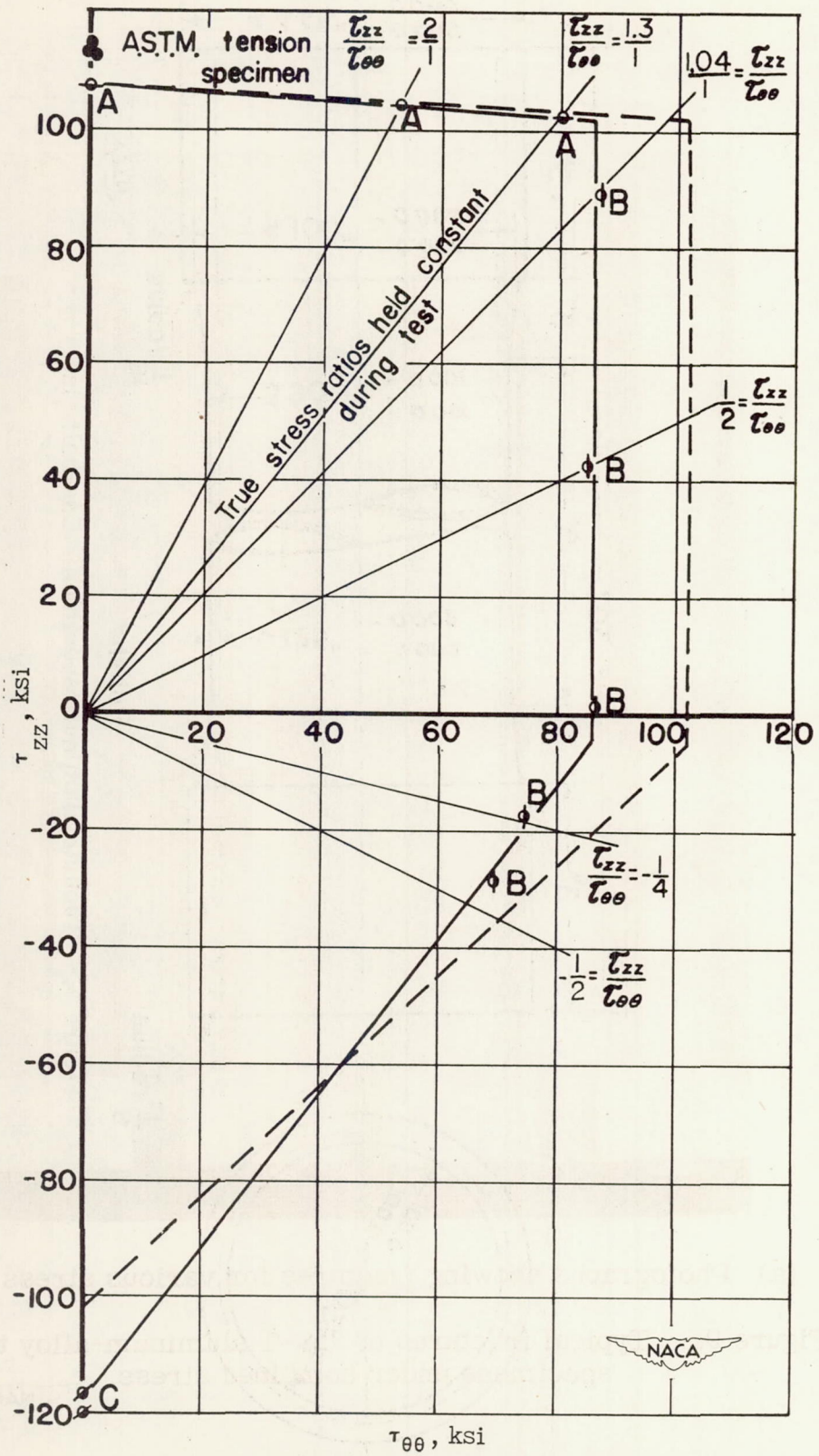

Figure 8.- True stress at fracture for 75S-T aluminum alloy.

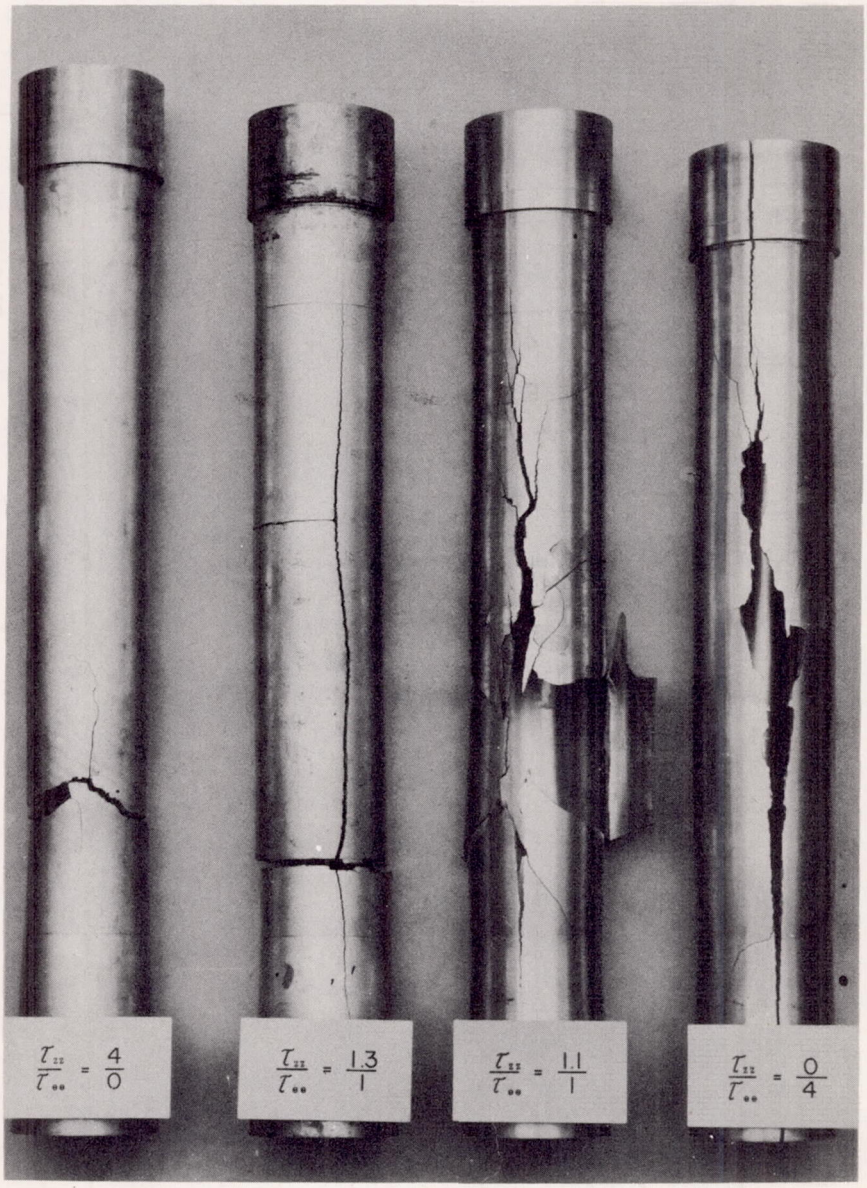

(a) Photographs showing fractures for various stress ratios.

Figure 9.- Typical fractures of 75S-T aluminum-alloy tubular specimens under combined stress.

Design-ation	Stress condition	Type of fracture
A	$\sigma_{xx} = \sigma_{yy}$	
B	$\sigma_{yy} = \sigma_{xx}$	
C	$\sigma_{yy} = 0 = \sigma_{xx}$	

Desig-nation	Stress condition	Type of fracture
A	$\tau_{zz} \geq \tau_{\theta\theta}$	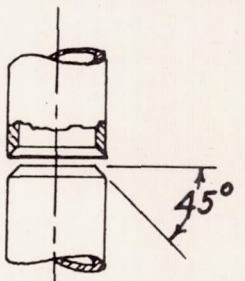
B	$\tau_{\theta\theta} \geq \tau_{zz}$	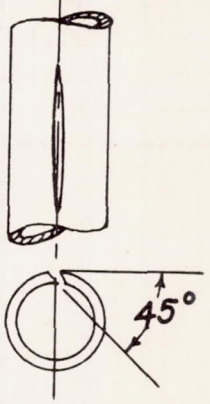
C	$\tau_{\theta\theta} \geq 0 \geq \tau_{zz}$	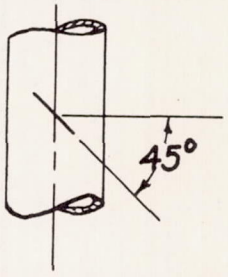

(b) Diagrammatic sketch of fracture planes in maximum shear direction.

Figure 9.- Concluded.

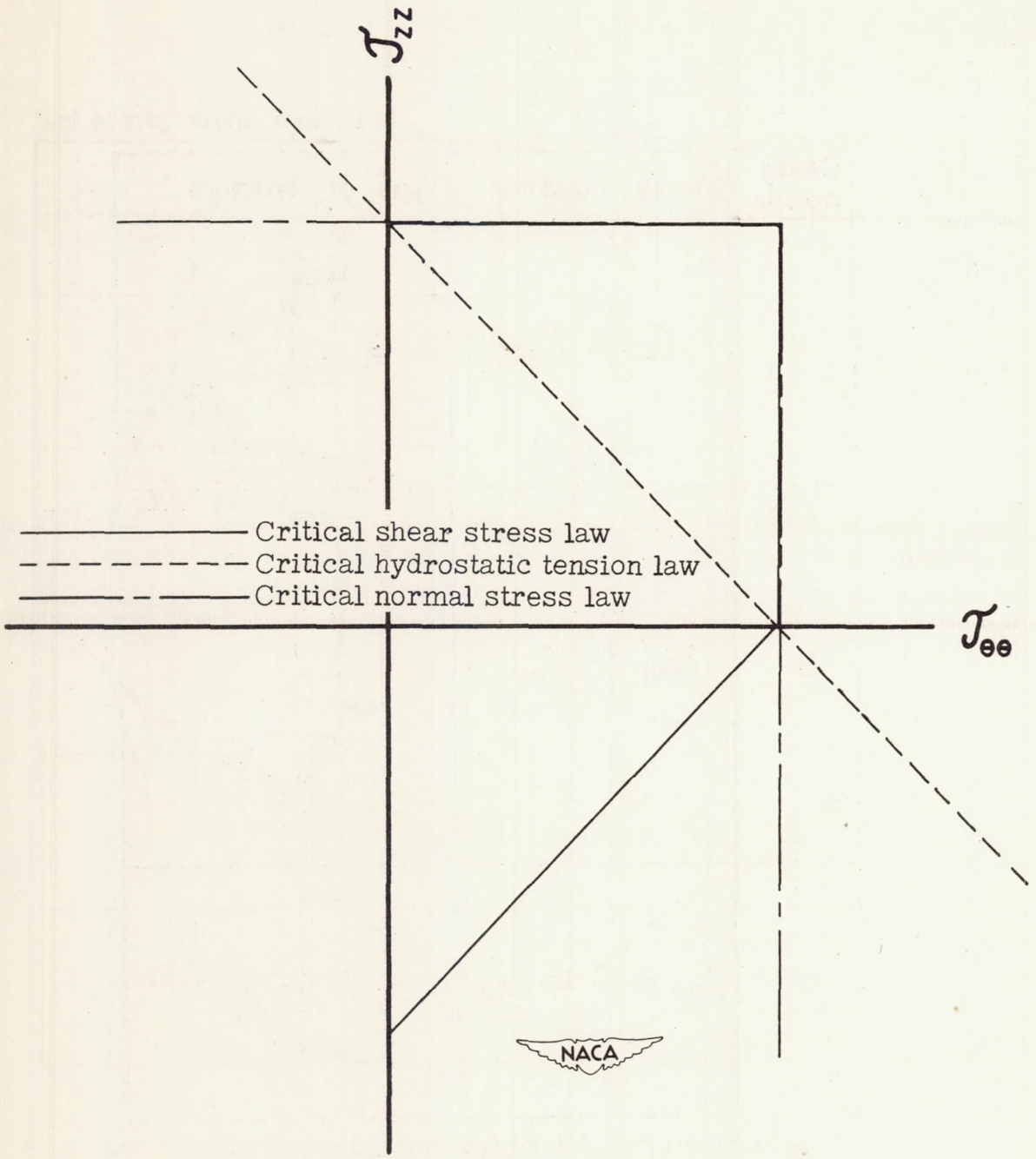

Figure 10.- Projection of fracture surfaces on $\tau_{zz}\,\tau_{\theta\theta}$ stress plane.

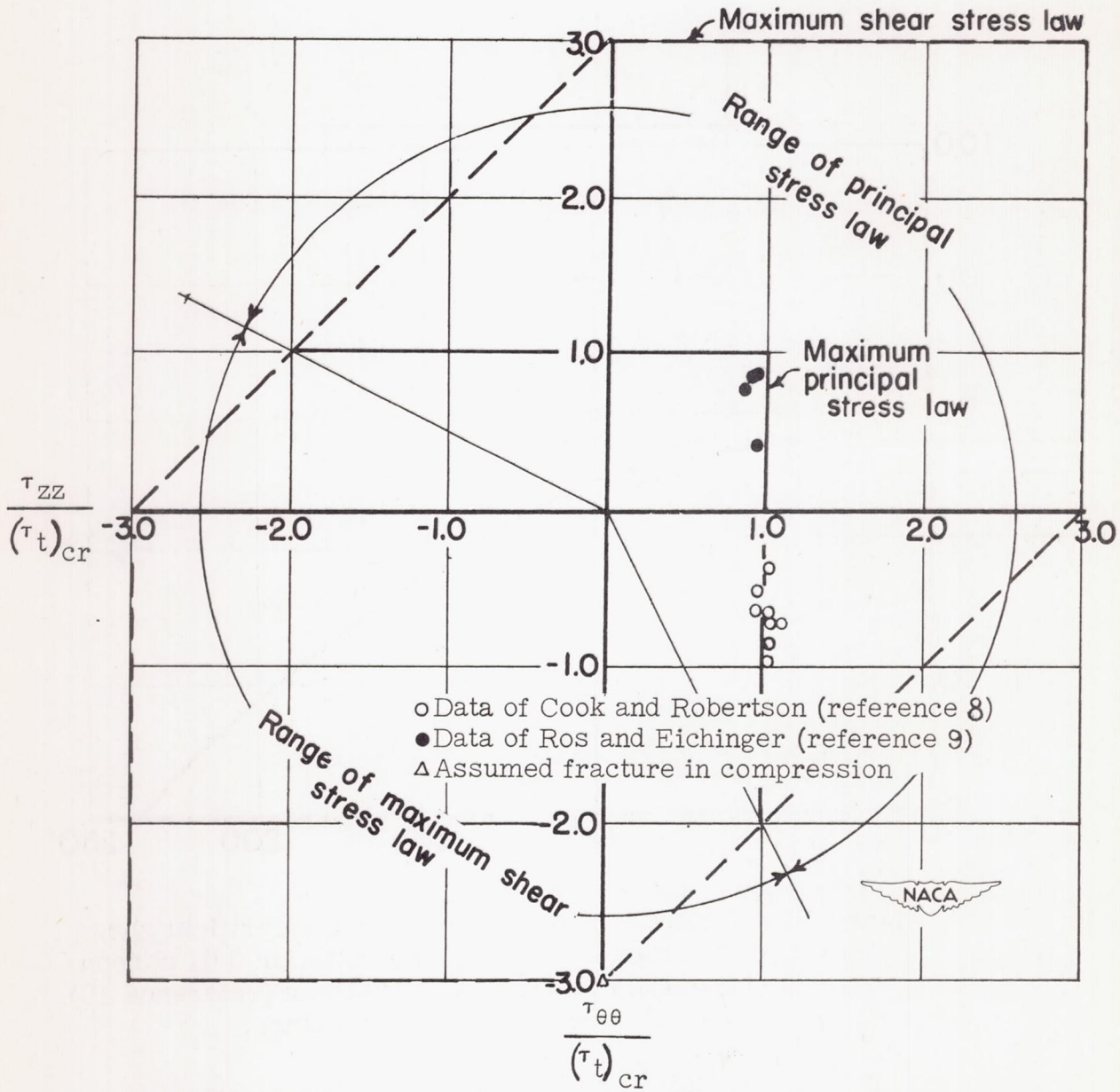

Figure 11.- Fracture of cast iron under biaxial stress. $(\tau_t)_{cr}$, critical fracture stress in simple tension.

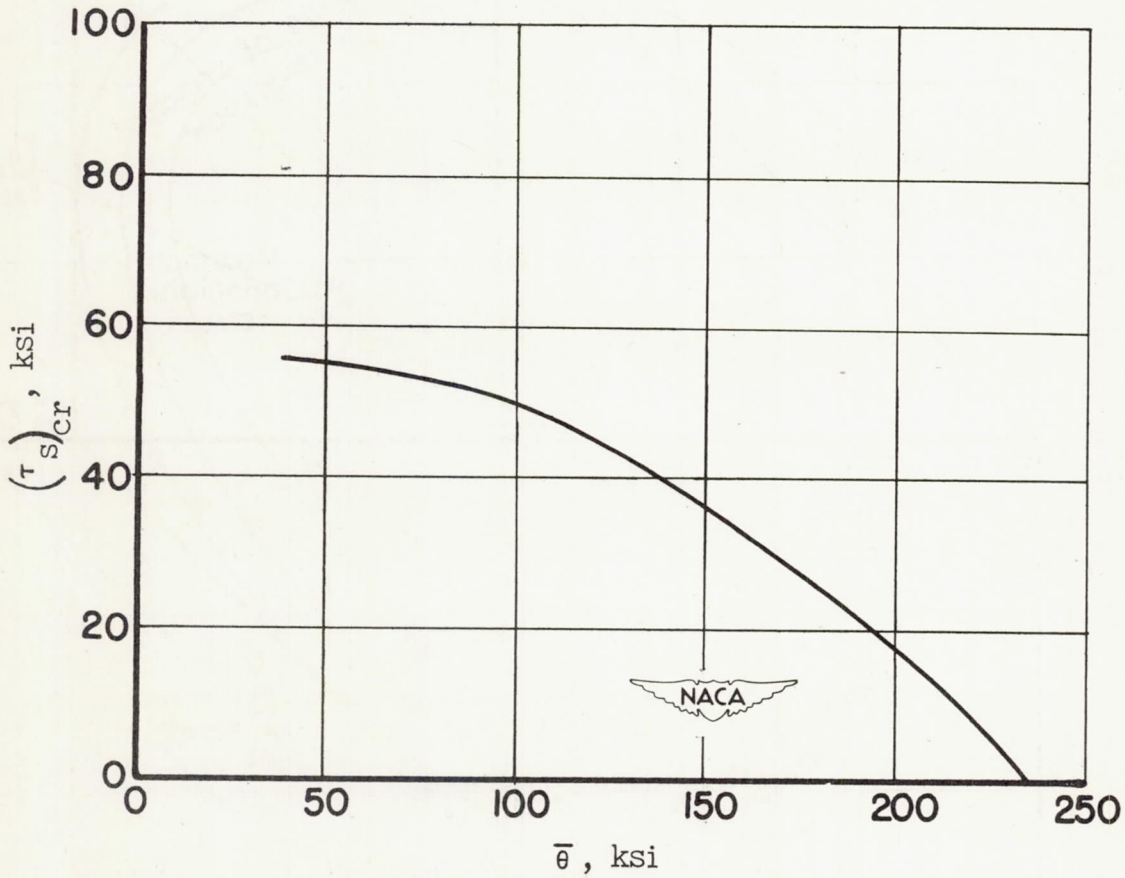

Figure 12.- Effect of hydrostatic tension on critical shear stress for fracture. Notched-bar tests for 0.61 carbon steel (cold-worked). Data from McAdam (reference 10).
$(\tau_s)_{cr}$, critical shear stress for fracture;

$\bar{\theta} = \frac{\tau_{11} + \tau_{22} + \tau_{33}}{3}$, mean hydrostatic tension.

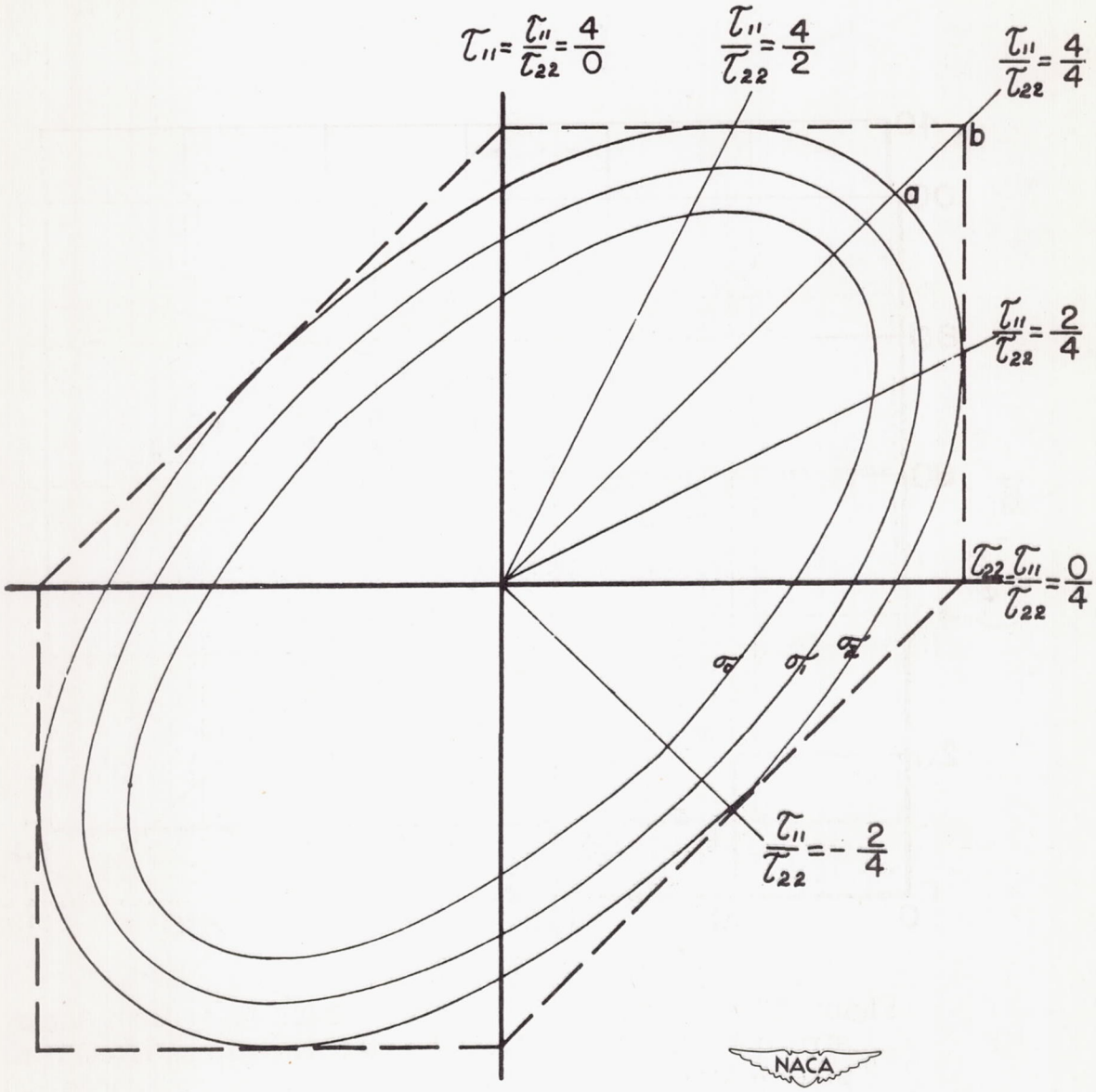

Figure 13.- Flow stress and fracture stress.

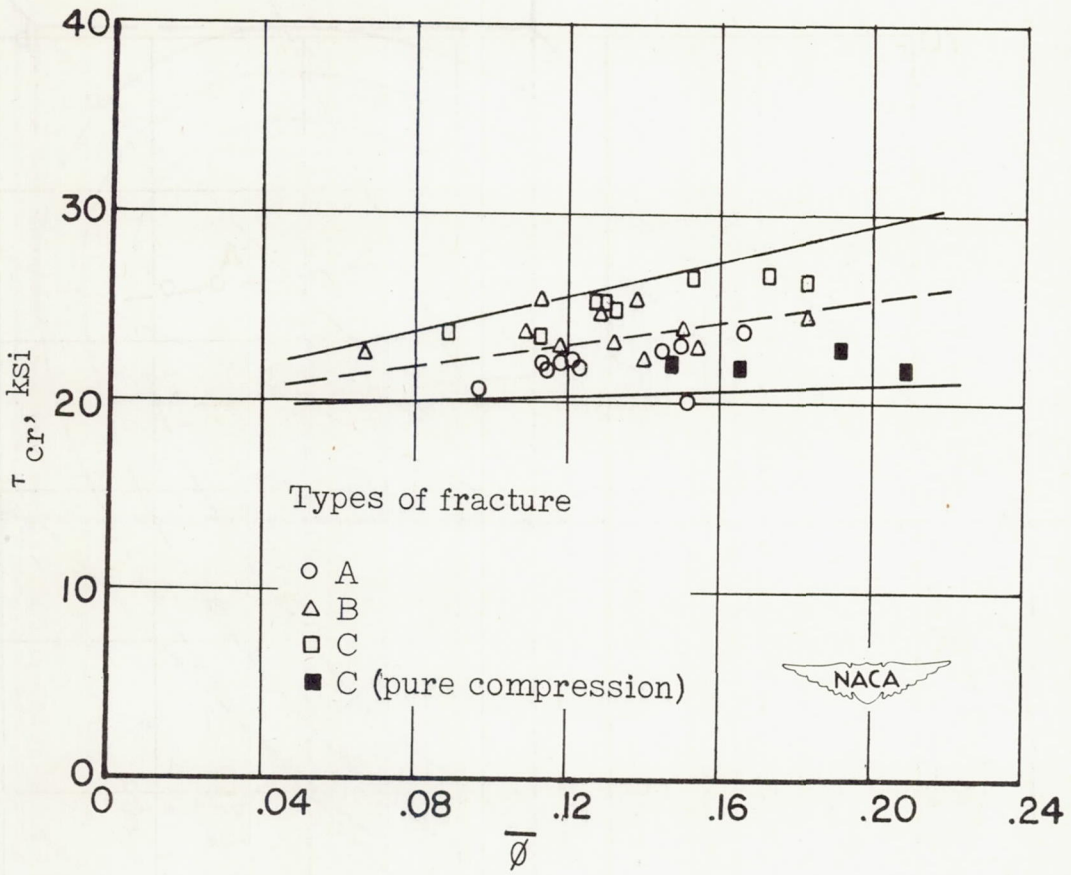

Figure 14.- Effect of effective strain $\overline{\phi}$ on shear stress at fracture for J-1 magnesium-alloy extrusion.

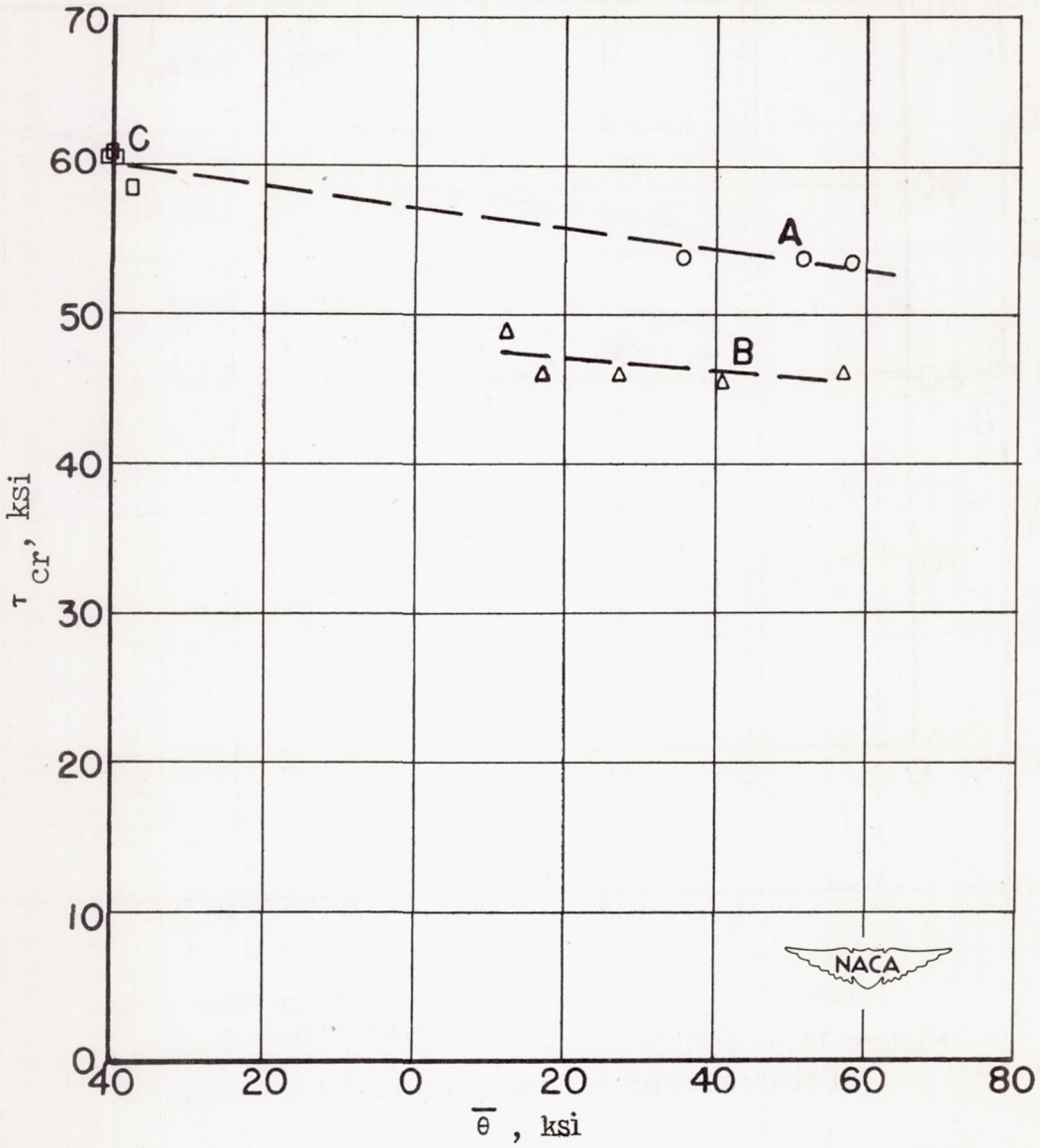

Figure 15.- Effect of hydrostatic tension $\bar{\theta}$ on shear stress at fracture for 75S-T aluminum alloy.

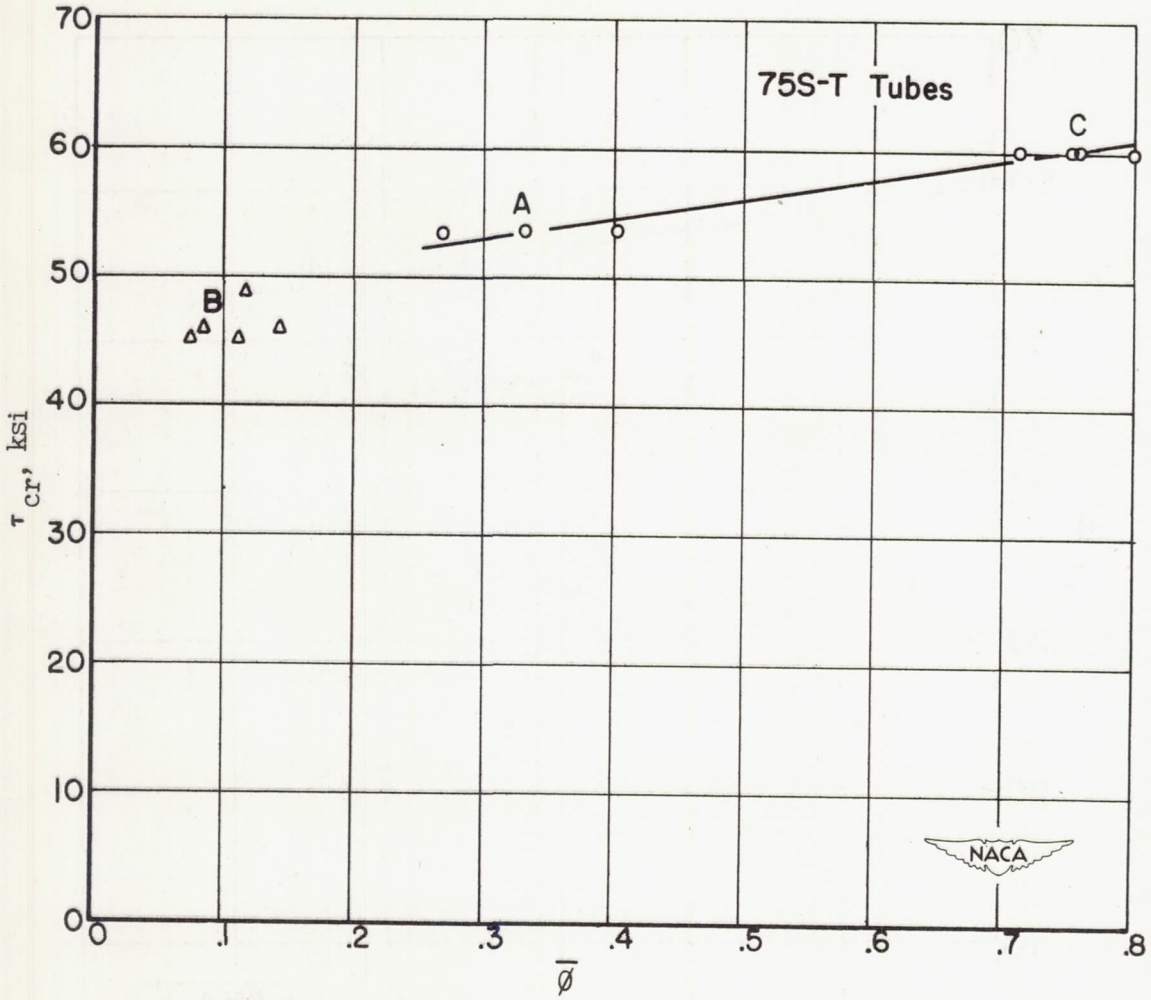

Figure 16.- Effect of effective strain $\bar{\phi}$ on shear stress at fracture for 75S-T aluminum alloy.